

A Malmquist-like bias in the inferred areas of diamond caustics and the resulting bias in inferred time delays for gravitationally lensed quasars

DEREK BALDWIN ¹ AND PAUL L. SCHECHTER ^{1,2}

¹*MIT Department of Physics
Cambridge, MA 02139, USA*

²*MIT Kavli Institute for Astrophysics and Space Research
Cambridge, MA 02139, USA*

ABSTRACT

Quadruply lensed quasars are visible only when the source quasar lies within the diamond caustic of the lensing galaxy. This condition creates a Malmquist-like selection effect in the population of observed quadruply lensed quasars, increasing the true caustic area. The inferred areas are therefore biased low by an amount proportional to the square of the uncertainty in the natural logarithm of the area, $\sigma_{\ln A}$. The inferred time delays, τ , vary with the caustic area of the lensing galaxy as \sqrt{A} . As a consequence, model time delays are biased low, leading to underestimates of the Hubble constant. Classical Malmquist bias also plays a role, with inferred magnifications biased low. As magnification is strongly anti-correlated with the area of the caustic, this classical Malmquist bias has an effect opposite to, but smaller than, the effect of the area bias. The overall effect is estimated to be small (median bias of less than 1%), but has the potential to be larger. Current posterior plots do not include caustic area, which limits the capability to accurately estimate the bias. With anticipated increases in sample sizes (in particular with the completion of LSST), correction for these biases becomes increasingly important.

Keywords: galaxies: quasars — gravitational lensing: strong, Malmquist bias, time delay cosmography

1. INTRODUCTION

The “era of precision cosmology” (e.g. [Kaplinghat & Turner 2001](#)) was widely heralded by cosmologists (but not all; see [Bridle et al. 2003](#)) and the occasional astronomer. Much of the precision in “precision cosmology” can be attributed to the high degree of homogeneity and small amplitude of perturbations in the early universe. But in today’s universe the populations of astronomical objects used for cosmological inference (e.g. Cepheid variable stars, type Ia supernovae, gravitationally lensed quasars) exhibit wide ranges of properties that must be taken into full account. These properties introduce uncertainties that become all the more important with the ever-increasing precision of our cosmological measurements. The present paper discusses

systematic biases in the measurements of several quantities associated with gravitational lenses (specifically caustic area, time delay, and magnification) that depend on these uncertainties.

We consider time delay measurements of quadruply lensed quasars, touted as a high precision method of measurement for the Hubble constant, H_0 ([Refsdal 1964](#); [Treu & Marshall 2016](#); [Wong et al. 2020](#)). It is well-known that these systems have a “diamond” or “astroidal¹” caustic ([Ohanian 1983](#)), which gives rise to a “quad” of images only when the source quasar is located inside this caustic ([Finch et al. 2002](#)). We demonstrate that this condition leads to an analogue of the well-known Malmquist effect ([Malmquist 1922](#); [Binney & Merrifield 1998](#)), in which the true luminosities of stars in flux-limited samples are higher than inferred due

Corresponding author: Paul L. Schechter
schech@achernar.mit.edu

¹ We note that these caustics form perfect astroids only in special cases. The caustics considered here are almost, but not quite, stretched astroids.

to a selection bias in the sample. In §2 we show how a similar selection effect occurs in the study of quadruply-lensed quasars, leading to a systematic underestimate of the diamond caustic area with respect to the true mean. In §3, we estimate the magnitude of this bias from uncertainties in the measurements of the external convergences of seven systems.

While such an underestimate in the inferred caustic areas of lensing galaxies might seem benign, we argue in §4 that the area and associated relative time delay in the system are strongly correlated, and so such an underestimate of caustic area introduces an underestimate of the time delay for each system. We claim that this in turn creates a finite underestimate of the Hubble constant that must be accounted for when making precise measurements. In §5 we calculate an estimate for the bias in the Hubble constant. Finally, in §6, we explore the classical Malmquist bias introduced by uncertainties in the magnification.

The present paper serves to establish the existence of this systematic error rather than produce a definitive calculation of it (e.g. accounting for multiple correlated model parameters).

2. THE MALMQUIST-LIKE EFFECTS FOR LENS CAUSTIC AREAS

In the same way that uncertainties in the derived luminosities of stars cause the true luminosities of the stars in a magnitude-limited sample to be brighter than the derived luminosities, the uncertainties in the derived areas of lens caustics cause the true caustic area to be larger than the derived caustic areas. This is due to the fact that a quadruply-lensed quasar requires the source to be within the diamond caustic (Finch et al. 2002). The systems we see as “quads” are likely to have true astroidal caustic areas larger than inferred because lensing galaxies with true astroidal caustics that are 1 standard deviation larger than inferred are over-represented and lensing galaxies with true astroidal caustics that are 1 standard deviation smaller than inferred are under-represented. Since we select only systems with their source quasar located inside the diamond caustic, the probability that a system is included in a sample of “quads” is proportional to the true area of its caustic. This is illustrated in Figure 1.

The derivation here of the size of the effect is similar to the derivation of Malmquist’s effect in Binney & Merrifield (1998). We introduce a Gaussian distribution of systems with true caustic areas A about an inferred mean value A_{inf} . Then the contribution to the total number of observed quadruply-lensed systems, N , with

respect to area is given by:

$$dN = \frac{1}{\sqrt{2\pi\sigma_{\ln A}^2}} n \left(\frac{A}{A_{inf}} \right) e^{-\frac{(\ln A - \ln A_{inf})^2}{2\sigma_{\ln A}^2}} d(\ln A) \quad (1)$$

where n is a number density (numbers per steradian) and $\sigma_{\ln A}$ is the standard deviation in $\ln A$. The ratio A/A_{inf} gives the probability of observing a lens with true caustic area A relative to one with A_{inf} . Substituting $\exp(\ln A - \ln A_{inf})$ for A/A_{inf} we have

$$dN = \frac{1}{\sqrt{2\pi\sigma_{\ln A}^2}} n e^{-\frac{(\ln A - \ln A_{inf})^2}{2\sigma_{\ln A}^2}} + (\ln A - \ln A_{inf}) d(\ln A) \quad (2)$$

$$= \frac{1}{\sqrt{2\pi\sigma_{\ln A}^2}} n e^{-\frac{(\ln A - \ln A_{inf} - \sigma_{\ln A}^2)^2 + \sigma_{\ln A}^4}{2\sigma_{\ln A}^2}} d(\ln A) \quad (3)$$

$$= \frac{1}{\sqrt{2\pi\sigma_{\ln A}^2}} n e^{\frac{\sigma_{\ln A}^2}{2}} e^{-\frac{(\ln A - \ln A_{inf} - \sigma_{\ln A}^2)^2}{2\sigma_{\ln A}^2}} d(\ln A) \quad (4)$$

which is a new Gaussian distribution with a shifted peak at

$$\ln A_{peak} = \ln A_{inf} + \sigma_{\ln A}^2. \quad (5)$$

We can then define the “logarithmic area bias” that reflects this systematic error:

$$\Delta_{\ln A} \equiv \ln A_{inf} - \ln A_{peak} = -\sigma_{\ln A}^2. \quad (6)$$

The logarithmic mean of true caustic areas for lenses for which the inferred caustic area is A_{inf} is larger than inferred by $\sigma_{\ln A}^2$, or the inferred caustic areas are biased low by $\sigma_{\ln A}^2$. Similarly, Malmquist’s effect causes absolute magnitudes to be biased faint,

$$\Delta_M = M_0 - M_{peak} = 1.38\sigma_M^2, \quad (7)$$

where the factor of 1.38 is $\frac{3}{2} \ln 2.5$. In both cases, there is an additive bias in the logarithm of the relevant quantity – luminosity in the Malmquist case and caustic area for the quads – that is proportional to the square in the uncertainty in the logarithm of that quantity.

In the next section we explore how to estimate $\sigma_{\ln A}$.

3. ESTIMATING THE UNCERTAINTY IN CAUSTIC AREA

3.1. Background

The “effective”, 2D lensing potential, ψ , is given by

$$\psi(\vec{r}) = \frac{D_{ds}}{D_d D_s} \frac{2}{c^2} \int_0^\infty \Phi(D_d \vec{r}, z) dz \quad (8)$$

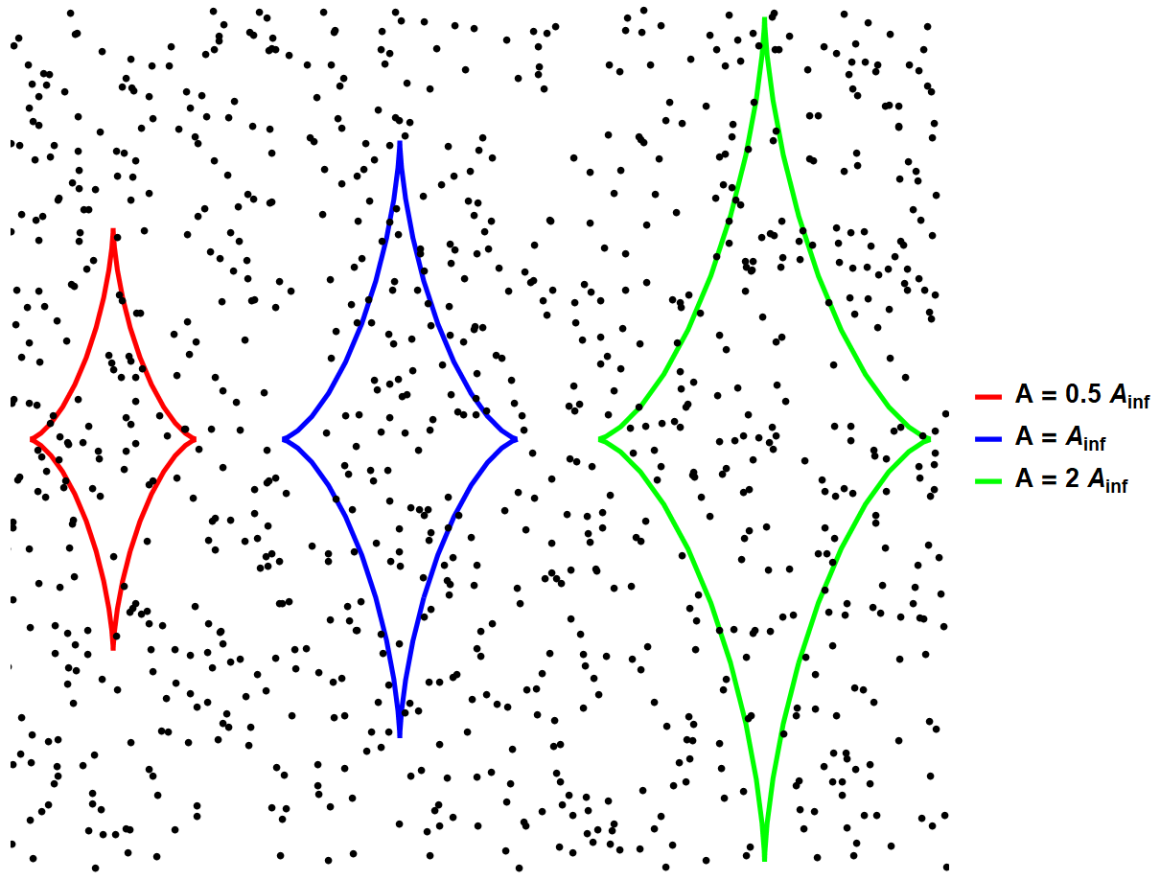


Figure 1. Plots of diamond caustics with areas $\ln A_{inf} \pm \sigma_{\ln A}$, where $\sigma_{\ln A} = \ln 2$, and randomly generated source quasar locations. Quads with higher caustic areas are over-represented in a sample because more source locations fall within the larger areas. The average caustic area in a sample of quads is $A_{peak} \approx 1.5A_{inf}$.

where D_{ds} , D_d and D_s are the angular diameter distances between the lens and the source, the distance between the lens and the observe, and the distance between the observer and the source, respectively. The Newtonian gravitational potential of the lens is Φ .

Typical of the potentials we consider here is the power-law potential subject to an external shear field,

$$\psi(r, \theta) = br^\alpha + \frac{\gamma r^2}{2} \cos 2\theta \quad (9)$$

where b gives the mass scale of the lens, α is the power-law slope of the lens, and γ is the strength of the external tidal shear.

The deflection of the image is given by:

$$\vec{r} - \vec{r}_s = \nabla \psi(\vec{r}), \quad (10)$$

where \vec{r} is the angular image position and \vec{r}_s is the angular source position (Bourassa & Kantowski 1975).

Each image has an associated time delay due to its varying path length. We define the time delay difference τ to be the largest difference in time delays between the 4 images in a quadruply-lensed quasar. Treu & Marshall

(2016) and Refsdal (1964) tell us that $\tau \propto 1/H_0$.

We later examine external convergences, and so we also consider the surface mass density of a lensing galaxy, defined by the projection of the lensing galaxy onto the plane perpendicular to the line-of-sight to the quasar. That is,

$$\Sigma(\vec{r}) = \int \rho(\vec{r}, z) dz \quad (11)$$

where Σ is the surface mass density, \vec{r} is the radial coordinate of the projected galaxy, z is the line-of-sight coordinate, and ρ is the conventional mass density profile of the lensing galaxy.

The dimensionless convergence, κ , is defined as a scaled version of the surface mass density,

$$\kappa(\vec{r}) = \frac{\Sigma}{\Sigma_{cr}}, \quad (12)$$

where Σ_{cr} is the critical surface mass density needed to produce multiple images,

$$\Sigma_{cr} = \frac{c^2}{4\pi G} \frac{D_s}{D_d D_{ds}}. \quad (13)$$

Here c and G are the conventional speed of light and Newtonian gravitational constant, respectively, and κ satisfies a dimensionless version of Poisson’s equation.

3.2. Dependence of caustic area on external convergence

The mass sheet degeneracy is well-known in the literature (see [Falco et al. 1985](#)). Here we explore some of its consequences with respect to caustic areas and time delays.

We follow the development of [Falco et al. \(1985\)](#) and [Schneider & Sluse \(2013\)](#). We consider a convergence of the form

$$\kappa'(\vec{r}) = \lambda\kappa(\vec{r}) + (1 - \lambda), \quad (14)$$

where κ , as usual, is the convergence characterizing the mass distribution of the lensing galaxy and λ is a dimensionless quantity. We now define the quantity

$$\kappa_{ext} = 1 - \lambda \quad (15)$$

which is called the external convergence in the literature. This makes the convergence

$$\kappa'(\vec{r}) = (1 - \kappa_{ext})\kappa(\vec{r}) + \kappa_{ext}. \quad (16)$$

According to [Schneider & Sluse \(2013\)](#), if we scale the source plane coordinates by $1 - \kappa_{ext}$, the observables in the image plane remained unchanged. This means that if we model a galaxy without including the external convergence and then include the external convergence after, the corrected coordinates \vec{x}_{corr} of the caustic curve are calculated from the inferred coordinates \vec{x}_{inf} by the equation:

$$\vec{x}_{corr} = \frac{\vec{x}_{inf}}{1 - \kappa_{ext}}. \quad (17)$$

We are left with the corrected caustic area

$$A_{corr} = \frac{A_{inf}}{(1 - \kappa_{ext})^2}. \quad (18)$$

3.3. Markov chain Monte-Carlo simulations

Logarithmic caustic area has not, until now, seemed sufficiently important to warrant its inclusion in lens modelers’ posterior plots (e.g. Figure 2 of [Birrer et al. 2020](#)). In its absence, we must infer $\sigma_{\ln A}$ from the uncertainties in other derived parameters. We urge investigators to include it in their MCMC simulations and posterior plots, obviating the need for calculations like those that follow.

3.4. Caustic area as a function of model parameters

We start with generic model parameters, α_i . The standard deviation in the natural logarithm of the area is given by

$$\sigma_{\ln A}^2 = \sum_i \sum_j \frac{\partial \ln A}{\partial \alpha_i} \frac{\partial \ln A}{\partial \alpha_j} \sigma_{ij}^2, \quad (19)$$

where σ_{ij}^2 is the covariance between i and j .

The covariances $\sigma_{ij}^2 = \rho(i, j)\sigma_i\sigma_j$, where $\rho(i, j)$ is the correlation coefficient, can be estimated from published posterior plots, but $A(\alpha_1, \dots, \alpha_i)$ is needed to proceed further. In what follows we examine this functional dependence for a few simple potentials, giving a sense of how it might vary for more realistic models.

3.4.1. Singular isothermal potential in an external shear field

[Finch et al. \(2002\)](#) give an expression for the caustic area of a singular isothermal potential in an external shear field,

$$\psi(r, \theta) = br + \frac{\gamma r^2}{2} \cos 2\theta, \quad (20)$$

and find

$$A = \frac{3\pi}{2} b^2 \frac{\gamma^2}{1 - \gamma^2}. \quad (21)$$

This is one of the few lensing potentials for which an exact analytic solution is possible and, by virtue of this fact, it avoids much of the complication that follows. It is a limiting case of the next potential we consider.

3.4.2. Singular isothermal elliptical potential in an external shear field

[Luhtarv et al. \(2021\)](#) consider the SIEP + XS model,

$$\psi(r, \theta) = b\sqrt{q_{pot}x^2 + \frac{y^2}{q_{pot}}} - \frac{\gamma}{2}(x^2 - y^2). \quad (22)$$

They arrive at the approximate expression

$$A \approx \frac{3\pi b^2}{2} (\gamma + 2\eta)^2, \quad (23)$$

where η is the semi-ellipticity, $q_{pot} = (1 - \eta)/(1 + \eta)$. We can rewrite this in terms of the “effective quadrupole,”

$$\Gamma_{eff} = \frac{\gamma + \eta}{1 + \gamma\eta}, \quad (24)$$

which is tightly constrained by the elongation of the image configuration. The parameter b , roughly the Einstein radius, θ_E , is also well constrained. This gives:

$$A \approx \frac{3\pi\theta_E^2}{2} (2\Gamma_{eff} - \gamma)^2. \quad (25)$$

The only poorly constrained parameter is then γ . Calculation of the uncertainty in $\ln A$ is straightforward because we need not consider covariances.

3.4.3. Power-law + external shear potential

We are interested in the power-law + external shear potential, given by equation (9). We calculate the approximate area of the diamond caustic for this case in Appendix A. For this potential the Einstein radius is given by $\theta_E = (b\alpha)^{1/(2-\alpha)}$, which gives

$$A \approx \frac{3\pi}{2} \theta_E^2 \gamma^2 \left(\frac{1}{1-\gamma^2} \right)^{\frac{1}{2-\alpha}}. \quad (26)$$

As noted previously, the Einstein radius is very well determined for any given system and so is relatively constant even as the slope is allowed to vary.

The covariance between the slope and external shear will enter the calculation of the uncertainty in the area. Some systems, such as PG1115+080 and HE0435-1223, have rings that can, in the absence of external convergence, determine the power-law slope. Thus one would expect a weak correlation between the slope and the external shear, which is supported by the posterior plots in Figures 8 and 13 of [Chen et al. \(2019\)](#). Other systems, however, do not have these rings to constrain the slope (e.g. WFI2033-4723). The external shear and power-law slope are thus more strongly correlated for these systems, which is reflected in the corner plot in [Rusu et al. \(2020\)](#) Figure 7.

The complications arising from correlated parameters leave us with no easy way to proceed with an estimate in area uncertainties, especially in the absence of published correlation coefficients and varying circumstances for each individual system. We thus forego such a calculation while once more urging modelers to include area in their posterior plots to permit straightforward calculations.

3.5. A special case: caustic area as a function of external convergence

Most investigators estimate the external convergence from counts of galaxies near the line of sight to lensed quasars. Were this strictly true, it would be possible to determine that part of the the uncertainty in the caustic area due to uncertainty in the uncertainty in κ_{ext} from equation (18). But in practice modelers (e.g. [Rusu et al. 2020](#); [Chen et al. 2019](#)) use the external shear derived from the lens model as an additional constraint on the external convergence.

While this makes sense – there is mass surface density associated with the same groups and clusters that produce the external shear – it introduces a covariance, not explicitly presented, between the two parameters. We nonetheless proceed to calculate caustic area uncertainties on the assumption that caustic areas do not depend

on other model parameters in order to obtain an estimate of the effect.

We examine the seven systems collected in [Birrer et al. \(2020\)](#) Figure 6. Using equation (18) we find the uncertainties in the logarithms of the areas due to the external shear as

$$\sigma_{\ln A} = \frac{d(\ln A)}{d\kappa_{ext}} \sigma_{\kappa_{ext}} \quad (27)$$

$$= \frac{2}{1-\kappa_{ext}} \sigma_{\kappa_{ext}}. \quad (28)$$

The confidence intervals for κ_{ext} are all lopsided, which is not consistent with our simplifying assumption of a Gaussian distribution. We approximate a Gaussian distribution by averaging the two bounds of the confidence interval to get an ad-hoc standard deviation. The approximate logarithmic area biases for these seven systems are listed in Table 1.

Table 1. External convergences and area biases for the seven systems in [Birrer et al. \(2020\)](#) Figure 6

System	κ_{ext}	$\Delta_{\ln A}$
B1608+656	$0.103_{-0.045}^{+0.084}$	$-2.1 \cdot 10^{-2}$
RXJ1131-1231	$0.069_{-0.026}^{+0.043}$	$-5.5 \cdot 10^{-3}$
HE0435-1223	$0.004_{-0.021}^{+0.033}$	$-2.8 \cdot 10^{-3}$
SDSS1206+4332	$-0.004_{-0.022}^{+0.036}$	$-3.3 \cdot 10^{-3}$
WFI2033-4723	$0.059_{-0.044}^{+0.077}$	$-1.7 \cdot 10^{-2}$
PG1115+080	$-0.006_{-0.021}^{+0.032}$	$-6.4 \cdot 10^{-3}$
DES0408-5354	$-0.040_{-0.024}^{+0.038}$	$-3.6 \cdot 10^{-3}$

3.6. Combining the effects of uncertainties in two uncorrelated parameters

Suppose that two uncorrelated model parameters, call them f and g , contribute to the uncertainty in caustic area. We take the propagating uncertainty in the logarithm of the area due to the uncertainty in f to be $\sigma_{\ln A, f}$. That is,

$$\sigma_{\ln A, f} = \frac{\partial \ln A}{\partial f} \sigma_f. \quad (29)$$

We similarly define the uncertainty in the log of the area due to the uncertainties in g to be $\sigma_{\ln A, g}$. We start with equation (1),

$$dN \propto \left(\frac{A}{A_{inf}} \right) e^{-\frac{(\ln A - \ln A_{inf})^2}{2\sigma_{\ln A}^2}} d(\ln A). \quad (30)$$

According to equation (19), we can express $\sigma_{\ln A}^2$ as

$$\sigma_{\ln A}^2 = \sigma_{\ln A, f}^2 + \sigma_{\ln A, g}^2 \quad (31)$$

for uncorrelated parameters $(\alpha_1, \alpha_2) = (f, g)$, because the covariance of two uncorrelated parameters is zero. Then

$$dN \propto \left(\frac{A}{A_{inf}} \right) e^{\frac{-(\ln A - \ln A_{inf})^2}{2(\sigma_{\ln A, f}^2 + \sigma_{\ln A, g}^2)}} d(\ln A). \quad (32)$$

The algebra in this scenario is the exact same as in §2 upon the substitution $\sigma_{\ln A}^2 = \sigma_{\ln A, f}^2 + \sigma_{\ln A, g}^2$, so we omit it. This gives an area bias of

$$\Delta_{\ln A}^{both} = A_{inf} - A_{peak} = -(\sigma_{\ln A, f}^2 + \sigma_{\ln A, g}^2) \quad (33)$$

for uncorrelated f and g .

3.7. Combining the effects of uncertainties in two perfectly correlated parameters

We now suppose that f and g are perfectly correlated parameters, following the exact same procedure. We again expand the $\sigma_{\ln A}^2$ term according to equation (19), with $(\alpha_1, \alpha_2) = (f, g)$. We then get

$$\sigma_{\ln A}^2 = \left(\frac{\partial A}{\partial f} \right)^2 \sigma_f^2 + 2 \frac{\partial A}{\partial f} \frac{\partial A}{\partial g} \sigma_f \sigma_g + \left(\frac{\partial A}{\partial g} \right)^2 \sigma_g^2 \quad (34)$$

$$= \left(\frac{\partial A}{\partial f} \right)^2 \sigma_f^2 + 2 \frac{\partial A}{\partial f} \frac{\partial A}{\partial g} \sigma_f \sigma_g + \left(\frac{\partial A}{\partial g} \right)^2 \sigma_g^2 \quad (35)$$

in the case of perfect correlation. Putting this in terms of $\sigma_{\ln A, f}$, defined in equation (29), and $\sigma_{\ln A, g}$, we are left with

$$dN \propto \left(\frac{A}{A_{inf}} \right) e^{\frac{-(\ln A - \ln A_{inf})^2}{2(\sigma_{\ln A, f} + \sigma_{\ln A, g})^2}}. \quad (36)$$

The algebra in this case is again the same as in §2 with the substitution $\sigma_{\ln A} = \sigma_{\ln A, f} + \sigma_{\ln A, g}$, so we don't repeat it. We arrive at

$$\ln A_{peak} = \ln A_{inf} + (\sigma_{\ln A, f} + \sigma_{\ln A, g})^2 \quad (37)$$

and

$$\Delta_{\ln A}^{both} = -(\sigma_{\ln A, f} + \sigma_{\ln A, g})^2. \quad (38)$$

4. THE EFFECT OF CAUSTIC AREAS ON TIME DELAYS

4.1. The effect of variable power-law slope on caustic areas and time delays

We examine 3 different systems that figure prominently in the TDCOSMO (Birrer et al. 2020) results: HE0435-1223, WFI2033-4723, and PG1115+080, and then analyze how varying diamond caustic areas influence the time delay. We adopt the power-law + external shear lensing potential of equation (9), as implemented in Keeton's `lensmodel` program (Keeton 2001).

4.1.1. Methodology

`lensmodel`'s times are non-dimensionalized, and the program assigns a standardized redshift to the lens and source in the absence of a specification (which is the case here).

1. For each of the 3 systems, we find the lens model that best fits the observations (image/galaxy position, image fluxes, etc.), all with a power-law slope (α) value of 1.
2. We then create fictitious "perfect twin systems" with image positions, fluxes, etc. altered to exactly match the simulated values from `lensmodel`. This removes uncertainties due to image/galaxy positions so as to isolate the effects of changing α on area.
3. We then create new models for each system with set α values of 0.5, 0.9, 1.0, 1.1, and 1.5. Each new model is generated with the "perfect twin" data values for the positions, fluxes, etc. This creates different-sized diamond caustics with areas given by equation (26).
4. We then find the time delays for each of these modeled systems. The caustic areas are calculated numerically from the curves generated by `lensmodel`.

4.1.2. Results

The results for each of the 3 systems are contained below in Table 2 and Figure 2.

Table 2. Areas and Time Delays for HE0435-1223, WFI2033-4723, and PG1115+080

	HE0435-1223		WFI2033-4723		PG1115+080	
α	A	τ	A	τ	A	τ
(Number)	(μ) ²	(Time)	(μ) ²	(Time)	(μ) ²	(Time)
(1)	(2)	(3)	(4)	(5)	(6)	(7)
0.5	0.0913	0.3544	0.305	0.9740	0.181	0.8048
0.9	0.0491	0.2605	0.170	0.7278	0.100	0.5975
1.0	0.0405	0.2370	0.140	0.6640	0.083	0.5444
1.1	0.0328	0.2134	0.113	0.5994	0.067	0.4909
1.5	0.0100	0.1187	0.036	0.3354	0.021	0.2739

We see in Figure 2 that all three cases have a straight line log-log plot with slope $0.5 \pm .01$. Without further

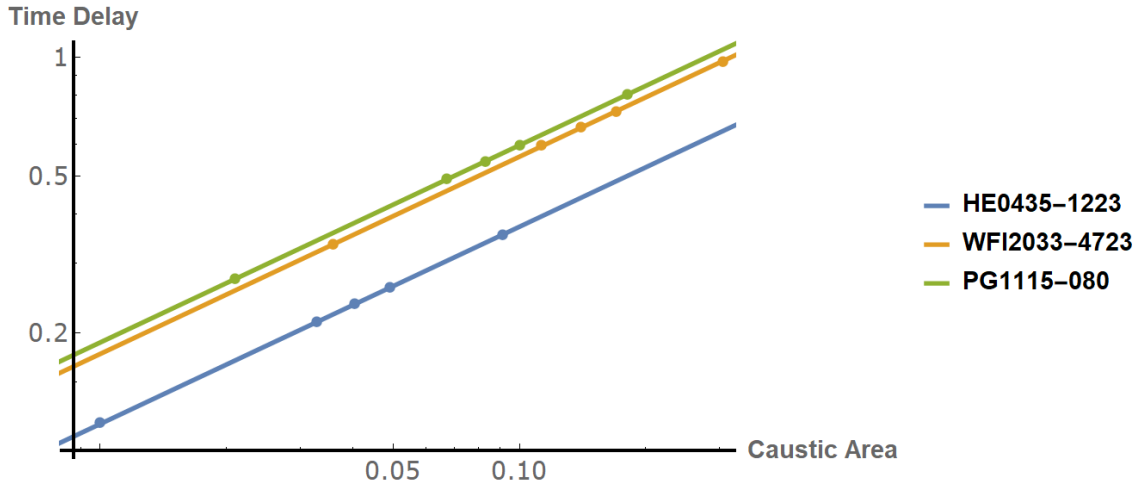


Figure 2. Log-Log Plots for Caustic Area (A) vs. Time Delay (τ) with lines of best fit. Each line of best fit has slope $\frac{1}{2}$.

proof, we shall assume that the time delay follows the relationship $\tau \propto \sqrt{A}$.

4.2. The effects of external convergences on time delays

For the specific case of external convergence, it is possible to show analytically that the time varies as the square root of the area. Birrer et al. (2016) tell us that the true time delay scales inversely with $1 - \kappa_{ext}$. That is,

$$\tau_{corr} = \frac{\tau_{inf}}{1 - \kappa_{ext}}, \quad (39)$$

where τ_{inf} is the inferred time delay, calculated ignoring line-of-sight mass effects.

Comparing with equation (18), we see that

$$\tau \propto \sqrt{A} \quad (40)$$

when varying κ_{ext} , the same relationship found in §4.1.2.

Together, these results allows us to use the biases in the area calculated in §3 to calculate the “logarithmic delay bias”, given by

$$\Delta_{\ln \tau} \equiv \frac{1}{2} \Delta_{\ln A} \quad (41)$$

or half of the logarithmic area bias. The delay biases for the three systems are given in Table 3.

5. THE EFFECT OF AREA BIAS ON THE HUBBLE CONSTANT

The negative bias in caustic area produces a negative bias in time delay. The Hubble constant is proportional to the ratio of the modeled time delay to the observed time delay. That is,

$$\frac{H_0^{inferred}}{H_0^{assumed}} = \frac{\tau_{mod}}{\tau_{obs}}, \quad (42)$$

where τ_{obs} is the observed time delay and τ_{mod} is the modelled time delay. If the modeled time delays are indeed biased low, the inferred Hubble constant will also be biased low.

Defining the bias in the logarithm of the Hubble constant to be:

$$\Delta_{\ln H_0} = \ln H_0 - \ln H_0^{inf}, \quad (43)$$

we have

$$\Delta_{\ln H_0} = \Delta_{\ln \tau}. \quad (44)$$

The logarithm of the Hubble constant is biased by the same amount as the modelled time delay.

We can use this result to roughly estimate percentage errors in the Hubble constant using the area biases in Table 1. These estimates are included in Table 3 below.

Table 3. Percent errors in the Hubble constant due to uncertainties in κ_{ext}

System	$\Delta_{\ln A}$	$\Delta_{\ln \tau}$	% Error in H_0
B1608+656	$-2.1 \cdot 10^{-2}$	$-1.1 \cdot 10^{-2}$	1.1%
RXJ1131-1231	$-5.5 \cdot 10^{-3}$	$-2.8 \cdot 10^{-3}$	0.3%
HE0435-1223	$-2.8 \cdot 10^{-3}$	$-1.4 \cdot 10^{-3}$	0.1%
SDSS1206+4332	$-3.3 \cdot 10^{-3}$	$-1.7 \cdot 10^{-3}$	0.2%
WFI2033-4723	$-1.7 \cdot 10^{-2}$	$-8.5 \cdot 10^{-3}$	0.9%
PG1115+080	$-6.4 \cdot 10^{-3}$	$-3.2 \cdot 10^{-3}$	0.3%
DES0408-5354	$-3.6 \cdot 10^{-3}$	$-1.8 \cdot 10^{-3}$	0.2%

These biases are in all cases quite small compared to the random uncertainties in the reported measurements of H_0 . But they should be treated as lower limits, as we have not assessed the effects of other parameters.

In the absence of covariances, their inclusion would increase the errors. Taking proper account of the covariances, however, might conceivably decrease the errors. We once again urge authors to include caustic areas in their posteriors to accurately capture the true magnitude of the bias, as the calculations become increasingly muddy when including more parameters and their correlations. We also caution authors that under- and/or over-estimates in parameter uncertainties can greatly affect the magnitudes of the time and area biases, as they grow as the *square* of said uncertainties.

6. THE EFFECT OF MAGNIFICATION ON SELECTION: MALMQUIST REDUX

6.1. Malmquist bias in mean magnification

In this section we examine the actual Malmquist bias by considering selection effects caused by uncertainties in the inferred magnification. We start with the Gaussian distribution of systems

$$dN \propto \left(10^{\beta \ln \mu}\right) e^{-\frac{(\ln \mu - \ln \mu_0)^2}{2\sigma_{\ln \mu}^2}} d(\ln \mu), \quad (45)$$

where μ is the magnification and $\sigma_{\ln \mu}$ is the uncertainty in the logarithm of magnification. The $10^{\beta \ln \mu}$ is meant to represent the increase in the surface density of quasars with decreasing flux, with a rate controlled by the generic parameter β . A reasonable value might be $\beta = 0.3$, roughly half the Euclidean expectation of $10^{0.6(2.5 \log \mu)}$, but we leave it to investigators to choose a value appropriate to the case at hand. It has the same effect as the A/A_{inf} term in §2, acting as a selection function. This expression is equivalent to

$$dN \propto \left(\frac{\mu}{\mu_0}\right)^{2.3\beta} e^{-\frac{(\ln \mu - \ln \mu_0)^2}{2\sigma_{\ln \mu}^2}} d(\ln \mu), \quad (46)$$

if $\ln 10$ is approximated as 2.3. We can then complete the square in the exponent and get the expression

$$dN \propto e^{-\frac{(\ln \mu - \ln \mu_0 - 2.3\beta\sigma_{\ln \mu}^2)^2}{2\sigma_{\ln \mu}^2}} d(\ln \mu). \quad (47)$$

This is another Gaussian distribution with a shifted average of

$$\ln \mu_{peak} = \ln \mu_0 + 2.3\beta\sigma_{\ln \mu}^2. \quad (48)$$

We can define yet another bias, the ‘‘magnification uncertainty bias²’’, as

$$\Delta_{\ln \mu} = \ln \mu_0 - \ln \mu_{peak} = -2.3\beta\sigma_{\ln \mu}^2. \quad (49)$$

² Magnification uncertainty bias is not to be confused with ‘‘magnification bias’’, the term introduced by Turner (1980) to explain why the ratio of lensed quasars to unlensed quasars is higher at brighter apparent magnitudes

This has the same form as the biases calculated above, and so carries the same unfortunate computational complications. We therefore urge that modelers include magnification in addition to caustic area in their posterior plots so as to accurately compute the uncertainties in the magnification.

6.2. Magnification and caustic area

Magnification is well known to be related to caustic area (e.g. Finch et al. 2002). The exact relation, however, changes depending on the model used. For lenses with superposed external convergence,

$$A \propto \mu^{-1}. \quad (50)$$

This is the case because the areas of both the caustic and source are multiplied by the same factor. We also claim without proof that this is a good approximation for lens profiles similar to equation (9), at least for slopes close to unity, as shown in Figure 3. This plot was created using the same method in §4.1, but this time with average magnification of the 4 images, μ , instead of τ .

In contrast, for the singular isothermal sphere with external shear, Finch et al. (2002) find

$$A \propto \mu^{-2}. \quad (51)$$

In both cases, the magnification is strongly correlated with the caustic area, and so we cannot compute the bias in the time delay as if they were uncorrelated.

For simplicity, we assume that the magnification and area are perfectly correlated. We proceed exactly as in §2, but adding the $10^{\beta \ln \mu}$ term in front of the Gaussian. With this term we have

$$dN \propto \left(10^{\beta \ln \mu}\right) \left(\frac{A}{A_{inf}}\right) e^{-\frac{(\ln A - \ln A_{inf})^2}{2\sigma_{\ln A}^2}} d(\ln A) \quad (52)$$

$$\propto \left(\frac{\mu}{\mu_0}\right)^{2.3\beta} \left(\frac{A}{A_{inf}}\right) e^{-\frac{(\ln A - \ln A_{inf})^2}{2\sigma_{\ln A}^2}} d(\ln A). \quad (53)$$

There are two cases to consider, $A \propto \mu^{-1}$ and $A \propto \mu^{-2}$. We first examine the former. Substituting in for the magnification in equation (53), we get

$$dN \propto \left(\frac{A}{A_{inf}}\right)^{1-2.3\beta} e^{-\frac{(\ln A - \ln A_{inf})^2}{2\sigma_{\ln A}^2}} d(\ln A), \quad (54)$$

from which we arrive at a logarithmic area bias of

$$\Delta_{\ln A}^{comb} = -(1 - 2.3\beta)\sigma_{\ln A}^2, \quad (55)$$

or, for our proposed value of $\beta = 0.3$,

$$\Delta_{\ln A}^{comb} = -0.31\sigma_{\ln A}^2. \quad (56)$$

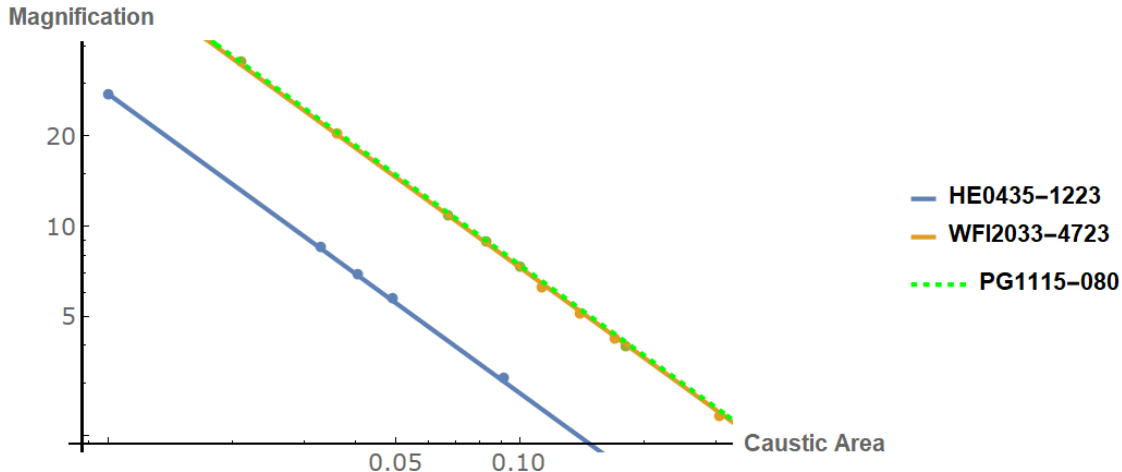


Figure 3. Log-Log Plots for Caustic Area (A) vs. Magnification (μ) with lines of best fit. Each line of best fit has slope -1 .

For the other case, $A \propto \mu^{-2}$, the calculation is the exact same following the substitution. We then get

$$\Delta_{\ln A}^{comb} = -(1 - 1.15\beta)\sigma_{\ln A}^2, \quad (57)$$

and

$$\Delta_{\ln A}^{comb} = -0.655\sigma_{\ln A}^2. \quad (58)$$

for $\beta = 0.3$. As before, these biases have an associated logarithmic time bias with magnitude one-half the area bias.

We note that the inclusion of the magnification works *against* the area bias and reduces it. The exact magnitude of the reduction is case-dependent, as the relationship between the area and magnification varies for each case. While we believe that $A \propto \mu^{-1}$ is a good approximation for lens profiles of the form of equation (9), we suggest that authors still investigate the area-magnification relation for their systems of interest to accurately measure this effect.

7. CONCLUSION

Due to the nature of the selection of quadruply lensed quasars in our analysis of lensing systems, it is inevitable that, on average, known quads have associated lensing galaxies with inferred caustic areas biased low with respect to the true caustic areas, because the cross section for quadruplicity is proportional to caustic area. A Malmquist bias due to the limiting magnitude of the survey produces a smaller bias in the caustic area that has the opposite sign. While it is in principle possible to compute an approximate correction for this selection effect from the uncertainties reported for the model parameters, in practice it requires too many simplifying assumptions. We therefore suggest that investigators report uncertainties in caustic areas in their analysis via MCMC simulations.

We claim that there is a straightforward relationship between the caustic area of a given system and its associated time delay, namely $\tau \propto \sqrt{A}$. A systematic bias in the caustic areas therefore entails a bias in the time delays measured in a given system. The Hubble constant is inversely proportional to the derived time delays in these systems, and so a bias low in area introduces a systematic underestimate in the value of the Hubble constant. We therefore claim that current measurements of the Hubble constant via the study of quadruply lensed quasars are biased low due to the over-representation of larger caustic areas in a sample.

Using reported uncertainties in estimated external convergences, we compute biases of less than 1%. Uncertainties in other model parameters may increase this. Of greatest concern, caustic area bias puts a premium on neither under- nor over-estimating uncertainties, as bias scales with the square of uncertainty.

ACKNOWLEDGEMENTS

We thank Drs. Philip Marshall, Sherry Suyu and Thomas Collett for comments on the manuscript. DB thanks the MIT UROP program for its support.

APPENDIX

A. APPROXIMATE CAUSTIC AREA FOR A POWER LAW + EXTERNAL SHEAR POTENTIAL

Here we follow closely the development in [Finch et al. \(2002\)](#) to derive an approximate analytic expression for astroidal caustic areas. We begin with the lensing potential:

$$\psi(r, \theta) = br^\alpha + \frac{\gamma r^2}{2} \cos 2\theta. \quad (\text{A1})$$

It will be easier to work with this in Cartesian form:

$$\psi(x, y) = b \left(\sqrt{x^2 + y^2} \right)^\alpha + \frac{\gamma (x^2 + y^2)}{2} \cos 2 \arctan \frac{y}{x} \quad (\text{A2})$$

$$= b \left(\sqrt{x^2 + y^2} \right)^\alpha + \frac{\gamma (x^2 + y^2)}{2} \left(\frac{x^2}{x^2 + y^2} - \frac{y^2}{x^2 + y^2} \right) \quad (\text{A3})$$

$$= b \left(\sqrt{x^2 + y^2} \right)^\alpha + \frac{\gamma}{2} (x^2 - y^2). \quad (\text{A4})$$

The astroidal caustic is where the inverse magnification matrix,

$$\mu^{-1} = \left(1 - \frac{\partial^2 \psi}{\partial x^2} \right) \left(1 - \frac{\partial^2 \psi}{\partial y^2} \right) - \left(\frac{\partial^2 \psi}{\partial x \partial y} \right) \quad (\text{A5})$$

disappears.

As for the shape of the caustic, according to [An & Evans \(2006\)](#), the “series [for the area] are also Taylor-series expansions with respect to γ at $\gamma = 0$. If we truncate the expansion of the caustic after [the first] term, the expression reduces to the equation of the tetra-cuspi-hypocycloid, or the astroid.” We make the simplifying assumption that $\gamma \ll 1$, so as to simplify the expression to that of approximately an astroid. The area of an astroid is given by

$$A = \frac{3\pi}{8} xy, \quad (\text{A6})$$

where x is the x -intercept of the caustic and y is the y -intercept ([Finch et al. 2002](#)). We then only consider the intercepts of the caustic in this calculation. On the axes, the cross term goes to zero so we can ignore it. We are then left with:

$$\mu^{-1} = \left(1 - b \left(\alpha \sqrt{x^2 + y^2}^{\alpha-1} \frac{y^2}{(x^2 + y^2)^{\frac{3}{2}}} + \alpha(\alpha - 1) \sqrt{x^2 + y^2}^{\alpha-2} \frac{x}{\sqrt{x^2 + y^2}} \right) - \gamma \right) \quad (\text{A7})$$

$$\times \left(1 - b \left(\alpha \sqrt{x^2 + y^2}^{\alpha-1} \frac{x^2}{(x^2 + y^2)^{\frac{3}{2}}} + \alpha(\alpha - 1) \sqrt{x^2 + y^2}^{\alpha-2} \frac{y}{\sqrt{x^2 + y^2}} \right) + \gamma \right). \quad (\text{A8})$$

On the x -axis, it is the second term that goes to zero. Thus the x -intercept solves the equation:

$$0 = 1 - b\alpha x^{\alpha-2} + \gamma, \quad (\text{A9})$$

giving us

$$x_c = \pm b^{\frac{1}{2-\alpha}} \left(\frac{\alpha}{1 + \gamma} \right)^{\frac{1}{2-\alpha}}. \quad (\text{A10})$$

A parallel calculation for the y -intercept gives us

$$y_c = \pm b^{\frac{1}{2-\alpha}} \left(\frac{\alpha}{1 - \gamma} \right)^{\frac{1}{2-\alpha}}. \quad (\text{A11})$$

Remapping back to the source plane via the lens equation,

$$\vec{r} - \vec{r}_s = \nabla \psi(\vec{r}), \quad (\text{A12})$$

we get

$$x_a = x_c (1 - b\alpha x_c^{\alpha-2} - \gamma) \quad (\text{A13})$$

$$= -2\gamma x_c \quad (\text{A14})$$

$$= \pm 2\gamma b^{\frac{1}{2-\alpha}} \left(\frac{\alpha}{1+\gamma} \right)^{\frac{1}{2-\alpha}}. \quad (\text{A15})$$

The same process for the y-intercept yields

$$y_c = \pm 2\gamma b^{\frac{1}{2-\alpha}} \left(\frac{\alpha}{1-\gamma} \right)^{\frac{1}{2-\alpha}}. \quad (\text{A16})$$

By the assumption $\gamma \ll 1$, we know the area of the caustic is proportional to the product of these two intercepts. The constant of proportionality for an astroid shape is $3\pi/8$. Thus we arrive at the final expression

$$A = \frac{3\pi}{2} \gamma^2 b^{\frac{2}{2-\alpha}} \left(\frac{\alpha^2}{1-\gamma^2} \right)^{\frac{1}{2-\alpha}}. \quad (\text{A17})$$

REFERENCES

- An, J. H., & Evans, N. W. 2006, *MNRAS*, 369, 317, doi: [10.1111/j.1365-2966.2006.10303.x](https://doi.org/10.1111/j.1365-2966.2006.10303.x)
- Binney, J., & Merrifield, M. 1998, *Galactic Astronomy* (Princeton University Press)
- Birrer, S., Amara, A., & Refregier, A. 2016, *JCAP*, 2016, 020, doi: [10.1088/1475-7516/2016/08/020](https://doi.org/10.1088/1475-7516/2016/08/020)
- Birrer, S., Shajib, A. J., Galan, A., et al. 2020, *A&A*, 643, A165, doi: [10.1051/0004-6361/202038861](https://doi.org/10.1051/0004-6361/202038861)
- Bourassa, R. R., & Kantowski, R. 1975, *ApJ*, 195, 13, doi: [10.1086/153300](https://doi.org/10.1086/153300)
- Bridle, S. L., Lahav, O., Ostriker, J. P., & Steinhardt, P. J. 2003, *Science*, 299, 1532, doi: [10.1126/science.1082158](https://doi.org/10.1126/science.1082158)
- Chen, G. C. F., Fassnacht, C. D., Suyu, S. H., et al. 2019, *MNRAS*, 490, 1743, doi: [10.1093/mnras/stz2547](https://doi.org/10.1093/mnras/stz2547)
- Falco, E. E., Gorenstein, M. V., & Shapiro, I. I. 1985, *ApJL*, 289, L1, doi: [10.1086/184422](https://doi.org/10.1086/184422)
- Finch, T. K., Carlivati, L. P., Winn, J. N., & Schechter, P. L. 2002, *ApJ*, 577, 51, doi: [10.1086/342163](https://doi.org/10.1086/342163)
- Kaplinghat, M., & Turner, M. S. 2001, *PhRvL*, 86, 385, doi: [10.1103/PhysRevLett.86.385](https://doi.org/10.1103/PhysRevLett.86.385)
- Keeton, C. R. 2001, arXiv e-prints, astro. <https://arxiv.org/abs/astro-ph/0102341>
- Luhtaru, R., Schechter, P. L., & de Soto, K. M. 2021, *ApJ*, 915, 4, doi: [10.3847/1538-4357/abfda1](https://doi.org/10.3847/1538-4357/abfda1)
- Malmquist, K. G. 1922, *Meddelanden fran Lunds Astronomiska Observatorium Serie I*, 100, 1
- Ohanian, H. C. 1983, *ApJ*, 271, 551, doi: [10.1086/161221](https://doi.org/10.1086/161221)
- Refsdal, S. 1964, *MNRAS*, 128, 307, doi: [10.1093/mnras/128.4.307](https://doi.org/10.1093/mnras/128.4.307)
- Rusu, C. E., Wong, K. C., Bonvin, V., et al. 2020, *MNRAS*, 498, 1440, doi: [10.1093/mnras/stz3451](https://doi.org/10.1093/mnras/stz3451)
- Schneider, P., & Sluse, D. 2013, *A&A*, 559, A37, doi: [10.1051/0004-6361/201321882](https://doi.org/10.1051/0004-6361/201321882)
- Treu, T., & Marshall, P. J. 2016, *A&A Rv*, 24, 11, doi: [10.1007/s00159-016-0096-8](https://doi.org/10.1007/s00159-016-0096-8)
- Turner, E. L. 1980, *ApJL*, 242, L135, doi: [10.1086/183418](https://doi.org/10.1086/183418)
- Wong, K. C., Suyu, S. H., Chen, G. C. F., et al. 2020, *MNRAS*, 498, 1420, doi: [10.1093/mnras/stz3094](https://doi.org/10.1093/mnras/stz3094)